$La_4Ti_5Si_{4-x}P_xO_{22}$ (x = 0, 1): A New Family of Two-Dimensional Solids. Synthesis and Structure of the First Member (m = 1) of the Mixed-Valence Titanium(III/IV) Oxosilicate Series, $La_4Ti(Si_2O_7)_2(TiO_2)_{4m}$

Shumin Wang and Shiou-Jyh Hwu*

Department of Chemistry, Rice University, P.O. Box 1892, Houston, Texas 77251

Received August 16, 1994[⊗]

A novel family of two-dimensional oxosilicate and mixed-oxosilicophosphate compounds, $La_4Ti_5Si_{4-x}P_xO_{22}$ (x = 0, 1), has been synthesized and structurally characterized. The X-ray single-crystal structure analysis shows that the x = 0 phase adopts a monoclinic lattice with a = 13.621(4) Å, b = 5.673(3) Å, c = 11.143(2) Å, β = 100.59(2)°; $C2/m$ (No. 12); Z = 2. The unit cell, a chevkinite type, consists of alternately stacked lanthanum titanium pyrosilicate, $La_4Ti(Si_2O_7)_2$, and single-layer (m = 1) titanium oxide, TiO_2 (rutile), slabs. The $La_4Ti_5Si_4O_{22}$ phase represents the first member (m = 1) of the mixed-valence lanthanum titanium(III/IV) oxosilicate series, $La_4Ti(Si_2O_7)_2(TiO_2)_{4m}$. This framework can be viewed as a rutile lattice that is sliced along the [110] plane at various thicknesses, m. The Ti−Ti distances across the shared octahedral edges in the rutile slab are uniformly spaced at 2.84 Å ($\equiv b/2$), in contrast to the distorted Ti−Ti distances observed in the higher member (m = 2) of the series. Four-probe resistivity measurements on pressed pellet samples of the bulk x = 0 and 1 phases show sharp increases in resistivity at 13 and 90 K, respectively, which can possibly be attributed to the bipolaron formation. The structure and electrical property correlation is briefly discussed.

Introduction

Over the years much attention has been devoted to the investigation of mixed-valence transition metal oxides possessing metal−insulator transitions. A number of interesting and technologically important physical phenomena are associated with metal−insulator transitions,[1−4] such as superconductivity, charge density waves (CDW), and magnetic ordering. The metal−oxygen−metal (M−O−M) and/or metal−metal (M−M) linkages of the transition metal oxide structures are common features observed in these oxide frameworks and are deemed important to the transport properties which are induced by conduction electrons. However, the origin of these unusual physical phenomena and the related behavior of electron−electron and electron−lattice interactions in metal oxide frameworks are not yet fully understood, due to the complex interactions that result from complicated solid state, extended lattices. Therefore, a low-dimensional compound with simplified electronic interactions is of interest to the mechanistic study of electrical conductivity in technologically important metallic oxides which include, but are not limited to, high-T_c superconductors.

During our systematic search for transition metal rich oxo compounds, as described previously,[5] a new quasi-two-dimensional lanthanum titanium(III/IV) oxosilicate, $La_4Ti_9Si_4O_{30}$, has been synthesized. This novel compound, similar to the mineral perrierite,[6] is structurally characterized by a quasi-two-dimensional framework consisting of alternately stacked slabs of lanthanum titanium disilicate, $La_4Ti(Si_2O_7)_2$, and double-layer titanium oxide, TiO_2 (rutile). The structural formula of the oxosilicate compound can be written as $La_4Ti(Si_2O_7)_2(TiO_2)_{4m}$, where m represents the thickness of the rutile layers. Subsequent studies have shown that the lower member (m = 1) of this series can also be prepared by a similar method: a high-temperature solid-state reaction employing molten $BaCl_2$ flux. The newly synthesized oxosilicates form a rare layered-type structure,[7] where the framework can be viewed as a rutile lattice that is sliced along the [110] plane by closed-shell, nonmagnetic slicate slabs.[8] Due to the intergrown nature of the transition metal oxide, TiO_2 in this case, and silicate, the oxo compound series is also interesting in the study of interfacial

[⊗] Abstract published in *Advance ACS Abstracts,* December 1, 1994.

(1) Goodenough, J. B. In *Progress in Solid State Chemistry*; Reiss, H., Ed., Pergamon Press: New York, 1971; Vol. 5, pp 145−399.
(2) Wilson, J. A. *Adv. Phys.* **1972**, *21*, 143−198.
(3) (a) *Chemistry of High-Temperature Superconductors*; Nelson, D. L., Whittingham, M. S., George, T. F., Eds.; ACS Symposium Series 351; American Chemical Society: Washington, DC, 1987. (b) *Chemistry of High-Temperature Superconductors II*; Nelson, D. L., George, T. F., Eds.; ACS Symposium Series 377; American Chemical Society: Washington, DC, 1988.
(4) (a) Canadell, E.; Whangbo, M.-H. *Inorg. Chem.* **1994**, *33*, 1864−8 and references cited therein (b) Greenblatt, M. *Chem. Rev.* **1988**, *88*, 31−53. (c) Schlenker, C.; Dumas, J. In *Crystal Chemistry and Properties of Materials with Quasi-One-Dimensional Structures. A Chemical and Physical Synthetic Approach*; Rouxel, J., Ed., D. Reidel Publishing Co.: Dordrecht The Netherlands, (1986; pp 135−77. (d) Banks, E.; Wold, A. In *Preparative Inorganic Reactions*; Jolly, W. L., Ed., Interscience: New York, 1968; Vol. 4, p 237. (e) Hagenmuller, P. In *Progress in Solid State Chemistry*; Reiss, H., Ed., Pergamon: New York, 1971; Vol. 5, p 71.
(5) (a) Wang, S.; Hwu, S.-J. *J. Am. Chem. Soc.* **1992**, *114*, 6920−2. (b) Wang, S. Ph.D. Dissertation, Rice University, 1993.
(6) Gottardi, G. *Am. Mineral.* **1960**, *45*, 1−14.
(7) In the binary systems associated with transition metal cations the layered-type structure is not as commonly seen in oxides as it is in halides and chalcogenides. This is because the oxide anion is not as polarizable as the halide and chalcogenide anions. It is interesting to see that the silicates, as well as the closely related phosphates, form tetrahedrally coordinated oxide anions that are bulky and possess flexible X−O (X = Si, P) bonds. This flexibility may facilitate essential polarizability that is responsible, in part, for the formation of layered-type compounds, such as the presently studied oxosilicate series.
(8) Compounds with quasi-low-dimensional structures, such as the oxide bronzes, show interesting anisotropic electrical and magnetic properties. However, the weak interchain or interlayer electron interaction, due to a small separation gap, often complicates the interpretation of observed physical phenomena. The oxosilicate compounds of this kind may rectify this situation because of the closed-shell, nonmagnetic nature of silicate anions. The title compound series may be the first examples of extended solids with three-dimensional frameworks that possess nearly ideal two-dimensional properties.

0020-1669/95/1334-0166$09.00/0

chemistry and bonding of SiO_2-based catalysts and thin film materials.

Compared to the niobium and tantanum oxosilicates,[9] only a limited number of low-dimensional oxosilicate compounds associated with the first row, early transition metal cations has been synthesized. Compounds discovered thus far have shown novel structural features; namely, one-dimensional $La_2Ti_2SiO_9$,[10] two-dimensional $[(RE)_4M(Si_2O_7)_2](MO_2)_{4m}$ series (RE = La, Nd, M = Ti and RE = La, M = V for $m = 1$; RE = La, M = Ti for $m = 2$),[5b] and polymorphs α- and β-$La_4Ti_9Si_4O_{30}$.[11] The crystal structure of $La_4Ti_5Si_4O_{22}$ is believed to be related to that of the mineral chevkinite, whose structure had not been determined until this study.[12] In this paper we present the synthesis and X-ray single-crystal structure of the novel $La_4Ti_5Si_4O_{22}$ oxosilicate as well as the substitutional chemistry and electrical property studies of the $La_4Ti_5Si_{4-x}P_xO_{22}$ ($x = 0, 1$) family.

Experimental Section

Synthesis. Black column crystals (< 10% yield) of $La_4Ti_5Si_4O_{22}$ were grown from the $BaCl_2$ flux containing a reaction mixture of $La_2O_3/Ti_2O_3/P_2O_5 = 0.30/2.40/0.30$ mmol. The high melting $BaCl_2$ salt (mp 963 °C) was added to the reactants in a mass ratio of 5:1 as a flux for crystal growth. The reaction mixture was sealed inside a fused silica ampule which had been carbon coated by the pyrolysis of acetone. It was heated at 1100 °C for ca. 20 days, followed by slow cooling at a rate of −25 °C/h to 800 °C, and then furnace cooled to room temperature. Single crystals were retrieved by washing the product with deionized water using a suction filtration method. Results from the structure solution and qualitative chemical analysis indicated that the compound contains the silicon cation, Si^{4+}, which was attributed to the incorporation of silica from the reaction ampule. A possible carbon-assisted oxosilicate formation reaction pathway was then proposed as expressed by the following unbalanced chemical equations:

$$La_2O_3 + 8Ti_2O_3 + P_2O_5 + xC + \text{excess } SiO_2 \text{ (fused silica)} \rightarrow [\text{"}LaPO_4\text{"} + Ti_2O_3 + xC + \text{excess } SiO_2] \rightarrow La_4Ti_5Si_4O_{22} + P_4 + xCO + \text{etc.}$$

The formation of a phosphate phase, $LaPO_4$ for example, was presumably an intermediate step towards the reduction reaction. A small amount of carbon (x) in the equations was thought to function as a reducing agent to reduce phosphate to elemental phosphorus at the "expense" of the fused silica resulting in the oxosilicate phase as a reaction byproduct.[13] At the elevated temperature, the carbon coating deteriorated and the quartz wall was exposed to the molten $BaCl_2$ flux, which allowed the above mentioned reactions to occur. As evidence for the proposed reaction mechanism, a parallel reaction without carbon coating was run and it yielded neither the oxosilicate nor red phosphorus.

Table 1. Crystallographic Data[a] for $La_4Ti_5Si_4O_{22}$

chem formula	$La_4Ti_5Si_4O_{22}$	fw	1259.45
a, Å	13.621 (4)	space group	$C2/m$ (No.12)
b, Å	5.673 (3)	T, °C	23
c, Å	11.143 (2)	λ, Å	0.71069
β, deg	100.59 (2)	ϱ_{calcd}, gcm^{-3}	4.94
V, Å^3	846.4 (5)	linear abs coeff, cm^{-1}	125.15
Z	2		
R^b	0.035		
$R_w{}^c$	0.060		

[a] The cell constants are refined in the monoclinic crystal system using 25 high-angle reflections ($30° \le 2\theta \le 40°$). [b] $R = \sum[|F_o| - |F_c|]/\sum|F_o|$. [c] $R_w = [\sum w[|F_o| - |F_c|]^2/\sum w|F_o|^2]^{1/2}$.

Polycrystalline samples of the $La_4Ti_5Si_{4-x}P_xO_{22}$ ($x = 0, 1$) family were synthesized after the single crystal structure of the $La_4Ti_5Si_4O_{22}$ phase had been determined. The stoichiometric mixtures of La_2O_3, Ti_2O_3, TiO_2, and SiO_2/P_2O_5 were heated at 1200 °C in a carbon-coated fused silica tube for 10 days and then slowly cooled (−1 °C/min) to room temperature. The carbon coating remained intact after this reaction. The black powder samples were subject to X-ray analysis at room temperature using a Phillips PW 1840 diffractometer equipped with Cu Kα radiation and a Ni filter. NIST (National Institute of Standards and Technology) silicon internal standard was mixed with the samples. The diffraction patterns obtained ($10° \le 2\theta \le 60°$) were indexed and refined by the least-squares program LATT.[14] The refined cell constants are in good agreement with those obtained from the single-crystal indexing (see Table 1):

	$x = 0$	$x = 1$
a (Å)	13.617(9)	13.553(5)
b (Å)	5.677(3)	5.652(3)
c (Å)	11.154(8)	11.119(8)
β (deg)	100.70(7)	100.70(5)
V (Å^3)	847.3(9)	836.9(8)
no. of indexed reflcns	20	21

It is noted that the decreased cell volume for the $x = 1$ phase is consistent with what is expected for the substitution of the smaller sized P^{5+} cations for Si^{4+}.

X-ray Single-Crystal Structure Determination. The crystal structure of $La_4Ti_5Si_4O_{22}$ was determined by the single-crystal X-ray diffraction technique. A black column crystal ,with the dimensions 0.40 × 0.10 × 0.08 mm, was selected for indexing and intensity data collection on a Rigaku AFC5S four circle diffractometer (Mo Kα, λ = 0.710 69 Å) equipped with a graphite monochrometer. The crystallographic data is summarized in Table 1. A total of 1117 reflections ($2\theta_{max} = 55°$) were collected from two octants ($+h, +k, \pm l$) of which 1041 unique reflections with $I > 3\sigma$ (I) were used for the structure determination. On the basis of the extinction conditions and the successful solution and structure refinement, the space group was determined to be $C2/m$ (No. 12). An absorption correction was applied based on three azimuthal scans (2θ = 14.39, 22.30, 29.02°). The atomic coordinates were found by the PATTERSON method using the program SHELXS-86.[15] The structural and thermal parameters were refined by full-matrix least-squares methods to $R = 0.035$, $R_w = 0.060$, and GOF = 1.82 based on F with 101 variables, using the TEXSAN

(9) (a) Choisnet, J.; Ngugen, N.; Groult, D.; Raveau, B. *Mater. Res. Bul.* **1976**, *11*, 887−94. (b) Serra, D. L.; Hwu, S.-J. *J. Solid State Chem.* **1992**, *101*, 32−40. (c) Crosnier, M. P.; Guyomard, D.; Verbaere, A.; Piffard, Y.; Tournoux, M. *J. Solid State Chem.* **1992**, *98*, 128−32. (c) Serra, D. L. Ph.D. Dissertation, Rice University, 1994.

(10) Benbertal, D.; Mosset, A.; Trombe, J. C. *Mater. Res. Bull.* **1994**, *29*, 47−54.

(11) The two polymorphs are α-$La_4Ti_9Si_4O_{30}$ (reported previously in ref 5a), a = 13.542(8) Å, b = 5.750(3) Å, c = 15.186(3) Å, and β = 110.94(2)°, and β-$La_4Ti_9Si_4O_{30}$, a = 13.521(2) Å, b = 5.743(3) Å, c = 14.236(3) Å, β = 95.42(2)°. These two structures are closely related; the silicate sublattices in the two structures are mirror images of each other, whereas the TiO_2 slab orientation is fixed. Intuitively, the formations of the α- and β- polymorphs are thermodynamically equivalent; the difference can be simply attributed to the alternation of lattice matching between the silicate and titanium oxide sublattices. It is noted that, despite the difference in c, the d_{001} spacing ($\equiv c \times \sin\beta$) is essentially the same, e.g., 14.18 and 14.17 Å, respectively.

(12) (a) Ito, J. *Amer. Miner.* **1967**, *52*, 1094−1109. (b) Ito, J.; Arem, J. E. *Am. Miner.* **1971**, *56*, 307−319. (c) The synthetic chevkinite and perrierite are considered polymorphs within certain chemical compositions. $M_2Pr_4Ti_3Si_4O_{22}$ (M = Mg, Ni), for example, crystallizes as perrierite at 900 °C in air and transform to chevkinite structure at elevated temperatures above 1070 °C. It is now understood that the two structures are similar in sublattice arrangement but differ in distortion of the TiO_6 octahedral chain in the rutile sublattice which results in a distinguishable monoclinic β angle, e.g., ~100° and ~113°, respectively.

(13) (a) This proposed reaction pathway is based upon the general industrial procedure that produces red phosphorus. In the reaction ampule, the red phosphorus was found at the end away from the flux. (b) *Inorganic Chemistry*, 2nd ed.; Shriver, D. E.; Atkins, P., Langford, C. H., Eds.; W. H. Freeman and Co.: New York, 1994; p 508.

(14) LATT: Takusagawa, F. Ames Laboratory, Iowa State University, Ames, IA, unpublished research, 1981.

(15) Sheldrick, G. M. In *Crystallographic Computing 3*; Sheldrick, G. M., Krüger, C., Goddard, R., Eds.; Oxford University Press: London, 1985; pp 175−189.

Table 2. Atomic Coordinates and Thermal Parameters[a] for $La_4Ti_5Si_4O_{22}$

atom	Wyckoff notation	x	y	z	B_{eq}, Å^2
La(1)	4*m*	0.14372(3)	0	0.25964(4)	0.57(3)
La(2)	4*m*	0.43046(3)	0	0.25476(4)	0.64(3)
Ti(1)	2*c*	0	0	0.5	0.46(7)
Ti(2)	4*e*	0.25	0.25	0	0.47(5)
Ti(3)	2*b*	0.5	0	0	0.64(7)
Ti(4)	2*a*	0	0	0	0.58(7)
Si(1)	4*m*	0.3608(2)	0	0.5442(2)	0.48(7)
Si(2)	4*m*	0.2040(2)	0	0.7302(2)	0.44(8)
O(1)	4*m*	0.0923(4)	0	0.6573(5)	0.9(2)
O(2)	8*j*	0.0705(3)	0.2642(8)	0.4134(4)	0.9(1)
O(3)	8*j*	0.2232(3)	0.2387(7)	0.8131(3)	0.8(1)
O(4)	4*m*	0.1496(4)	0	0.0180(5)	0.5(2)
O(5)	4*m*	0.3554(4)	0	0.0261(6)	0.7(2)
O(6)	8*j*	0.4795(3)	0.2484(8)	0.8680(3)	0.7(1)
O(7)	4*m*	0.3116(4)	0	0.4036(5)	0.8(2)
O(8)	4*m*	0.2835(4)	0	0.6400(6)	1.3(2)

[a] Anisotropically refined atoms are given in the form of the isotropic equivalent displacement parameters defined as $B_{eq} = (8\pi^2/3)$ trace **U**.

software package.[16] The final positional and isotropic thermal parameters are given in Table 2.

Four-Probe Resistivity Measurements. DC four-probe resistivity measurements were made on pressed pellet samples with the dimensions ~0.2 × 3.1 × 12.1 mm. The pellets were sintered at 900−950 °C for 2−3 days in a fused silica ampule under vacuum. The pellet samples were fixed to the glass template with Apiezon grease to assure good thermal contact. Four Cu wires (0.25 mm diameter) were attached to the pellet with silver paste. The sample was placed on a copper-block sample mount in the cold head of a Janis closed-cycle refrigerator system, Model CCS 150, equipped with a LakeShore 330 temperature controller. Prior to the measurements, the sample chamber was evacuated under a rough pump to ca. 10^{-4} Torr . The current was supplied by a Keithley 182 current source, and the voltage was measured by a Keithley 220 digital nanovoltmeter. A 10 mA current was employed in the temperature range from 300 K to the lowest possible temperature where voltage can be read: 10 and 80 K for the $x = 0$ and 1 phases, respectively. Ohmic behavior was verified in both cases with a room-temperature $I-V$ curve. Contributions of the thermoelectric power to the voltage were calibrated by changing the direction of the current for each temperature measurement. The resistivity, ϱ, was calculated according the formula $\varrho = RdF$, where $R(\Omega)$ $(=V/I)$ is the resistance, d is the thickness of the pellet, and F is the product of all correction factors for a collinear four-probe array.[17]

Results and Discussion

The $La_4Ti_5Si_4O_{22}$ oxosilicate structure consists of alternately stacked TiO_2 and $La_4Ti(Si_2O_7)_2$ slabs. By viewing the unit cell approximately along the *b* axis of the monoclinic lattice, as shown by the ORTEP[18] drawing in Figure 1, a layered structure is discerned. The quasi-two-dimensional layered framework is characterized by the extended Ti−O bonds (drawn in thick lines) of the single-layer titanium oxide slab. The coordination geometries of the cations are shown in solid lines except for the lanthanum atoms for clarity. The four crystallographically independent titanium atoms, three (Ti(2)−Ti(4)) in the TiO_2 slab and one (Ti(1)) in the $La_4Ti(Si_2O_7)_2$ slab, adopt a

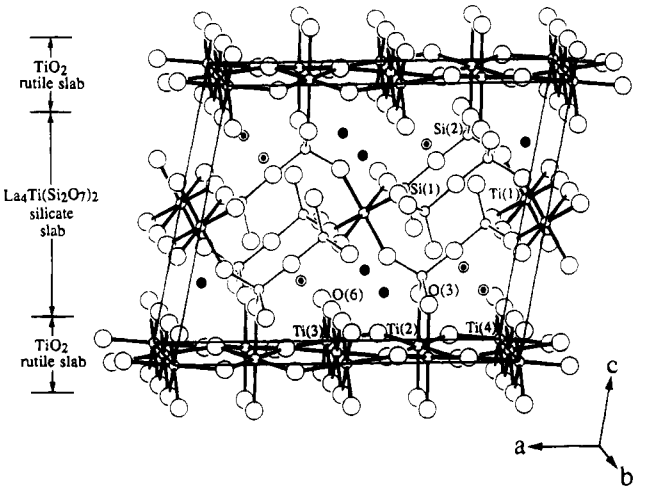

Figure 1. Structure of $La_4Ti_5Si_4O_{22}$ viewed approximately along the b axis of the monoclinic unit cell, as outlined. All the octahedral coordinations in TiO_6 are represented by thick lines and the tetrahedral coordinations in Si_2O_7 by thin lines. Small circles represent titanium and silicon atoms and large circles represent oxygen atoms, whereas small dotted and solid circles represent the two crystallographically independent lanthanum atoms, La(1) and La(2), respectively. Only two oxygen atoms, O(3) and O(6), are labeled for clarity.

six-coordination geometry with respect to the oxygen atoms. The fused TiO_6 units share opposite edges along the [010] direction forming octahedral chains and share corners along the [100] direction. In the $La_4Ti(Si_2O_7)_2$ silicate slab, $Ti(1)O_6$ and Si_2O_7 pyrosilicate (disilicate) units share corner oxygen atoms to form an open framework structure with the lanthanum atoms situated in the space near the interface. The interfacial oxygen atoms, O(3) and O(6), are shared by the two crystallographically independent lanthanum atoms.

Alternatively, the layered structure can be viewed as formed via lattice matching instead of van der Waals gaps. In the middle of the unit cell in Figure 1, a $Ti(1)O_6$ centered silicate slab is presented where each TiO_6 shares each of its six corner oxygen atoms with a Si_2O_7 pyrosilicate unit. The intergrowth of the above mentioned TiO_2 and $La_4Ti(Si_2O_7)_2$ slabs can be explained in the following manner. The pyrosilicates function as bulky ligands to "chelate" the titanium oxide slabs through the apical oxygen atoms, O(3), of the $Ti(2)O_6$ octahedra in the TiO_2 slab. The chelated and nonchelated octahedral chains are distorted cooperatively to facilitate the lattice matching. The octahedral-chain distortion is evidenced by the "bent" octahedra centered around the 2_1 axes at $x = 1/4$ and $3/4$ and the "twisted" octahedra around the 2-fold axes at $x = 0$ and $1/2$.

The layered structure can also be viewed as a rutile lattice that is sliced along the [110] plane by silicate slabs. The structural formula of the title compound can be written as $La_4Ti(Si_2O_7)_2(TiO_2)_4$. In the unit cell of the title compound, there are a total of eight titanium atoms in the rutile layer, which correlate to the titanium stoichiometry in the formula unit of $Z = 2$. The framework of the silicate slab is composed of one TiO_6 octahedron per six corner-shared Si_2O_7 pyrosilicate groups, accompanied by four lanthanum atoms giving rise to the structural formula $[La_4Ti(Si_2O_7)_2] \equiv [La_4Ti(Si_2O_7)_{6/3}]$. As the formula indicates, each pyrosilicate group is shared by three isolated titanium atoms, Ti(1). The Si_2O_7 groups are arranged in a parallel way with respect to their nearly linear, 177.9(4)°, Si−O−Si vectors forming channels where the lanthanum atoms reside. The structure of this 2-D oxosilicate is important in the sense that it consists of closed-shell, nonmagnetic Si_2O_7 groups, which not only structurally separate but also electronically insulate the TiO_2 slabs.

(16) (a) *TEXSAN: Single Crystal Structure Analysis Software, version 5.0*; Molecular Structure Corp.: The Woodlands, TX, 1989. (b) Scattering factors for non-hydrogen atoms: Cromer, D. T.; Waber, J. T. *International Table for X-ray Crystallography*; IV, Kynoch Press: Birmingham, 1974; Vol. IV, Table 2.2A, pp 71−98.
(17) *Quick Reference Manual for Silicon Integrated Circuit Technology*; Beadle, W. E., Tsai, J. C. C., Plummer, R. D., Eds.; John Wiley and Sons: New York, 1985.
(18) Johnson, C. K. ORTEP II. Report ORNL-5138. Oak Ridge National Laboratory, Oak Ridge, TN, 1976.

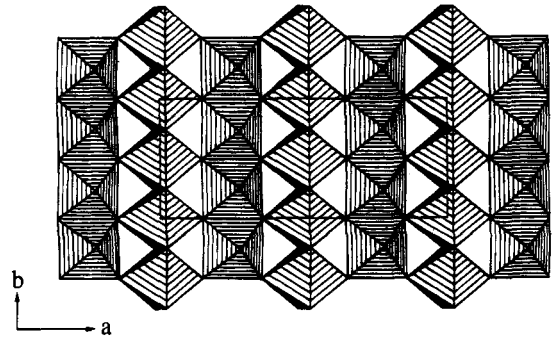

Figure 2. Polyhedral drawing of the rutile slab in $La_4Ti_5Si_4O_{22}$.

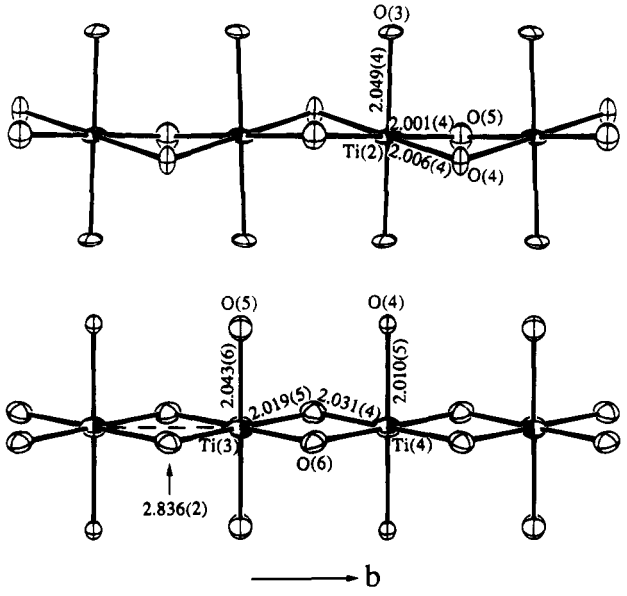

Figure 3. ORTEP drawing of the two octahedral chains: Ti(2) chain (top) and Ti(3)/Ti(4) chain (bottom). The anisotropic atoms are presented at 90% probability. The bond distances are in Å.

The TiO_2 slab structurally resembles the single-layer rutile framework where two sets of TiO_6 octahedral chains are in a parallel arrangement. As shown in Figure 2, the fused TiO_6 octahedra share opposite edges extending along the [010] direction, and also share corners with neighboring parallel chains along the [100] dimension. The corner-shared oxygen atoms between the parallel chains are three-coordinate with respect to the titanium atoms, a characteristic of the rutile structure. The octahedral chains are arranged such that the neighboring chains are approximately orthogonal to each other with respect to the 4-fold axes of the TiO_6 octahedra. The Ti−Ti distance across these shared octahedral edges has an uniform spacing of 2.84 Å, which is shorter than the 2.96 Å found in rutile and 3.02 Å, the critical distance for Ti−Ti interaction.[1,19] In the $m = 2$ α-phase, however, one set of the octahedral chains has an equally spaced Ti−Ti separation at the distance 2.88 Å and the other chain has alternating short (2.76 Å) and long (3.00 Å) distances. Although there is a minor difference in the arrangement of the rutile chains, the interslab interaction is the same in both $m = 1$ and 2 phases.

Despite the homogeneous Ti−Ti separation across the shared edge of the fused octahedra, these two TiO_6 octahedral chains are distorted in two distinct ways, shown in Figure 3. The two octahedral chains, Ti(2) chain (top) and the Ti(3)/Ti(4) chain (bottom), adopt different symmetries, e.g., the 2_1 and 2-fold axes along *b*, respectively. The pseudo 4-fold axes of the fused octahedra move toward (or away from) each other alternately in the Ti(2) chain, but they are twisted with respect to the *b* direction in the Ti(3)/Ti(4) chain. The degree of distortion is in part attributed to the bond strain occurring at the interface where the apical O(3) atoms are closely spaced because of the constraints of the small O(3)−Si(2)−O(3) tetrahedral bond angle. Consequently, the basal plans of the $Ti(2)O_6$ octahedra pucker. Subsequently, the cross-linked Ti(3)/Ti(4) chain, which shares O(4) and O(5), becomes twisted with respect to its 2-fold axes. The basal planes of the Ti(3)/Ti(4) chain remain horizontal. In both cases the TiO_6 octahedra are slightly distorted; this can be seen in the bond distances and angles shown in Table 3. The Ti−O coordinations show four short and two long Ti−O distances for the $Ti(2)O_6$ and $Ti(3)O_6$ octahedra and two short and four long for the $Ti(4)O_6$ octahedron. This octahedral distortion is consistent with the Jahn−Teller effect expected for the d^1 electronic configuration of the Ti^{3+} cation, based on the charge distribution assignment $[La_4Ti^{4+}(Si_2O_7)_2](TiO_2)_4^{4-}$ (see later discussion). The observed values describing the geometries of the TiO_6 octahedra, as well as the above mentioned Si_2O_7 pyrosilicate, are normal and comparable with those reported previously.[9a,20]

The coordination geometry of the two crystallographically independent LaO_8 polyhedra can be best described as a bicapped trigonal prism (btp). In Figure 4 (1 × La(1)O_8 and 2 × La(2)O_8), three btps are viewed down the triangular faces of the prism, so that the descriptive geometry and their connectivity are revealed. The polyhedra are made of oxygen atoms other than O(1) and O(8), which are the bridging atoms for Ti(1)−O(1)−Si(2) and Si(1)−O(8)−Si(2), respectively. The La(1)O_8 and La(2)O_8 btps share the common edge, O(2) and O(6), of the trigonal prisms, while the two symmetry related LaO_8 btps are separated. The La−O bond distances are relatively diverse, in that the six apical La−O distances of the trigonal prisms are in the range 2.45−2.61 vs 2.45−2.70 Å for La(1)O_8 vs La(2)O_8, respectively; the two capping La−O distances are 2.54/2.71 and 2.52/2.57 Å. The observed irregular La−O bond interaction suggests the lanthanum atoms are off-centered with respect to the trigonal prism. It is interesting to note, however, that the averaged La−O distances for the LaO_8 btps are almost identical, e.g., 2.57 Å and 2.56 Å, respectively, which is consistent with the sum of the Shannon crystal radii,[21] 2.58 Å, of eight coordinated La^{3+} (1.30 Å) and O^{2-} (1.28 Å).

The lanthanum titanium silicate slab, $La_4Ti(Si_2O_7)_2$, can be considered to be a charge reservoir relative to the titanium oxide slab. Intuitively, the electropositive cations, La^{3+} and Si^{4+}, in the silicate slab facilitate two possible sites for cation substitution, to fine tune the electronic structure of the rutile slab. The chemical modification through partial substitution of P^{5+} for Si^{4+} in the $La_4Ti_5Si_4O_{22}$ parent compound has successfully yielded the mixed-oxosilicophosphate phase, $La_4Ti_5Si_3PO_{22}$. The latter results in a modification of electron count at the valence region (see below). On the basis of the formal oxidation states adopted by the ions La^{3+}, Si^{4+}, and O^{2-}, there are over all four Ti d-electrons in each formula unit of the $La_4Ti_5Si_4O_{22}$ oxosilicate. Every mole of phosphorus substitution increases the electron count by one electron per formula unit, i.e., 5 e's per $La_4Ti_5Si_3PO_{22}$. The formation of the mixed-oxosilicophosphate compound, in theory, gives additional empirical merit to the investigation of electronic properties as a function of valence electrons that are associated with two-dimensional titanium oxide array.

(19) Goodenough, J. B. *Bull. Soc. Chim. Fr.* **1965**, 1200−1206.

(20) (a) Wang, S.; Hwu, S.-J. *J. Solid State Chem.* **1991**, *90*, 31−41. (b) Wang, S.; Hwu, S.-J. *Chem. Mater.* **1992**, *4*, 589−95.

(21) Shannon, R. D. *Acta Crystallogr.* **1976**, *A32*, 751−67.

Table 3. Important Bond Distances (Å) and Angles (deg) for $La_4Ti_5Si_4O_{22}$[a]

		TiO_6 Octahedra	
$Ti(1)^a-O(1)^{a,c'}$	1.960(6) (2×)	$Ti(2)^a-O(3)^{a',g'}$	2.049(4) (2×)
$Ti(1)^a-O(2)^{a,b,c,d'}$	2.107(4) (4×)	$Ti(2)^a-O(4)^{a,g}$	2.006(4) (2×)
$Ti(2)^a-O(5)^{a,g}$	2.001(4) (2×)		
$Ti(3)^a-O(5)^{a,c'''}$	2.043(6) (2×)	$Ti(4)^a-O(4)^{a,c}$	2.010(5) (2×)
$Ti(3)^a-O(6)^{a',b''',c'',d''}$	2.019(4) (4×)	$Ti(4)^a-O(6)^{e''',f'',h''',g'}$	2.031(4) (4×)
$O(1)^a-Ti(1)^a-O(1)^{c'}$	180	$O(3)^{a'}-Ti(2)^a-O(3)^{g'}$	180
$O(1)^a-Ti(1)^a-O(2)^{a,b}$	98.0(2) (2×)	$O(3)^{a'/g'}-Ti(2)^a-O(4)^{a/g}$	94.7(2) (2×)
$O(1)^a-Ti(1)^a-O(2)^{c',d'}$	82.0(2) (2×)	$O(3)^{a'/g'}-Ti(2)^a-O(4)^{a'/g'}$	85.3(2) (2×)
$O(1)^{c'}-Ti(1)^a-O(2)^{a,b}$	82.0(2) (2×)	$O(3)^{a'/g'}-Ti(2)^a-O(5)^{a/g}$	96.6(2) (2×)
$O(1)^{c'}-Ti(1)^a-O(2)^{c',d'}$	98.0(2) (2×)	$O(3)^{a'/g'}-Ti(2)^a-O(5)^{g/a}$	83.4(2) (2×)
$O(2)^a-Ti(1)^a-O(2)^{c'}$	180	$O(4)^a-Ti(2)^a-O(4)^g$	180
$O(2)^{a/b}-Ti(1)^a-O(2)^{d'/c'}$	89.3(2) (2×)	$O(4)^{a/g}-Ti(2)^a-O(5)^{a/g}$	88.2(2) (2×)
$O(2)^{a/c'}-Ti(1)^a-O(2)^{b/d'}$	90.7(2) (2×)	$O(4)^{a/g}-Ti(2)^a-O(5)^{g/a}$	91.8(2) (2×)
$O(2)^b-Ti(1)^a-O(2)^{d'}$	180	$O(5)^a-Ti(2)^a-O(5)^g$	180
$O(5)^a-Ti(3)^a-O(5)^{c'''}$	180	$O(4)^a-Ti(4)^a-O(4)^c$	180
$O(5)^a-Ti(3)^a-O(6)^{a',c'''}$	95.5(2) (2×)	$O(4)^a-Ti(4)^a-O(6)^{e'''/f''}$	94.2(2) (2×)
$O(5)^{c'''}-Ti(3)^a-O(6)^{c'',d''}$	95.5(2) (2×)	$O(4)^a-Ti(4)^a-O(6)^{h'''/g'}$	85.7(2) (2×)
$O(5)^a-Ti(3)^a-O(6)^{c'',d''}$	84.5(2) (2×)	$O(4)^c-Ti(4)^a-O(6)^{e'''/f''}$	85.7(2) (2×)
$O(5)^a-Ti(3)^a-O(6)^{a',d'''}$	84.5(2) (2×)	$O(4)^c-Ti(4)^a-O(6)^{h'''/g'}$	94.2(2) (2×)
$O(6)^{a'/c''}-Ti(3)^a-O(6)^{b''''/d''}$	88.5(2) (2×)	$O(6)^{e'''/h''}-Ti(4)^a-O(6)^{f''/g'}$	89.3(2) (2×)
$O(6)^{a'/b'''}-Ti(3)^a-O(6)^{d''/c''}$	91.4(2) (2×)	$O(6)^{e'''/f''}-Ti(4)^a-O(6)^{h'''/g'}$	90.7(2) (2×)
$O(6)^{a'/b'''}-Ti(3)^a-O(6)^{c''/d''}$	180 (2×)	$O(6)^{e'''/f''}-Ti(4)^a-O(9)^{g'/h'''}$	180 (2×)
$Ti(2)^a-Ti(2)^{b,b'}$	2.836(2) (2×)	$Ti(3)^a-Ti(4)^{g'}$	2.836(2) (2×)
$Ti(2)^{a,b}-O(4)^a-Ti(4)^a$	133.4(1) (2×)	$Ti(2)^a-O(4)^a-Ti(2)^b$	90.0(2)
$Ti(2)^{a,b}-O(5)^a-Ti(3)^a$	131.6(2) (2×)	$Ti(2)^a-O(5)^a-Ti(2)^b$	90.3(2)
$Ti(3)^{a''}-O(6)^a-Ti(4)^{e''}$	88.9(2)		
		SiO_4 Tetrahedra	
$Si(1)^a-O(2)^{g'/h'''}$	1.652(4) (2×)	$Si(2)^a-O(1)^a$	1.588(6)
$Si(1)^a-O(7)^a$	1.587(6)	$Si(2)^a-O(3)^{a,b}$	1.633(4) (2×)
$Si(1)^a-O(8)^a$	1.631(6)	$Si(2)^a-O(8)^a$	1.606(6)
$O(2)^{h'''}-Si(1)^a-O(2)^{g'}$	108.2(3)	$O(1)^a-Si(2)^a-O(3)^{a,b}$	109.1(2) (2×)
$O(2)^{h''',g'}-Si(1)^a-O(7)^a$	113.4(2) (2×)	$O(1)^a-Si(2)^a-O(8)^a$	111.9(3)
$O(2)^{h''',g'}-Si(1)^a-O(8)^a$	102.3(2) (2×)	$O(3)^a-Si(2)^a-O(3)^b$	112.1(3)
$O(7)^a-Si(1)^a-O(8)^a$	116.2(3)	$O(3)^{a,b}-Si(2)^a-O(8)^a$	107.3(2) (2×)
$Si(1)^a-O(8)^a-Si(2)^a$	177.9(4)		
		LaO_8 Polyhedra	
$La(1)^a-O(2)^{a,b}$	2.608(4) (2×)	$La(2)^a-O(2)^{e',f}$	2.704(4) (2×)
$La(1)^a-O(3)^{g',h''}$	2.585(4) (2×)	$La(2)^a-O(3)^{g',h''}$	2.562(4) (2×)
$La(1)^a-O(4)^a$	2.708(6)	$La(2)^a-O(5)^a$	2.565(6)
$La(1)^a-O(6)^{g',h'''}$	2.450(4) (2×)	$La(2)^a-O(6)^{c'',d''}$	2.445(4) (2×)
$La(1)^a-O(7)^a$	2.541(6)	$La(2)^a-O(7)^a$	2.521(6)

[a] Symmetry codes: (a) x, y, z; (b) $x, -y, z$; (c) $-x,-y, -z$; (d) $-x, y, -z$; (e) $1/2 + x, 1/2 + y, z$; (f) $1/2 + x, 1/2 - y, z$; (g) $1/2 - x, 1/2 - y, -z$; (h) $1/2 - x, 1/2 + y, -z$; (a') $x, y, -1 + z$; (b') $x, 1 - y, z$; (c') $-x, -y, 1 - z$; (d') $-x, y, 1 - z$; (e') $1/2 + x, -1/2 + x, z$; (f') $-1/2 + x, 1/2 - y, z$; (g') $1/2 - x, 1/2 - y, 1 - z$; (h') $1/2 - x, -1/2 + y, -z$; (a'') $x, y, 1 + z$; (b'') $x, -y, -1 + z$; (c'') $1 - x, -y, 1 - z$; (d'') $1 - x, y, 1 - z$; (e'') $1/2 + x, 1/2 + y, 1 + z$; (f'') $-1/2 + x, 1/2 - y, -1 + z$; (h'') $1/2 - x, -1/2 + y, 1 - z$; (c''') $1 - x, -y, -z$; (e''') $-1/2 + x, -1/2 + y, -1 + z$; (h''') $1/2 - x, -1/2 + y, 1 - z$.

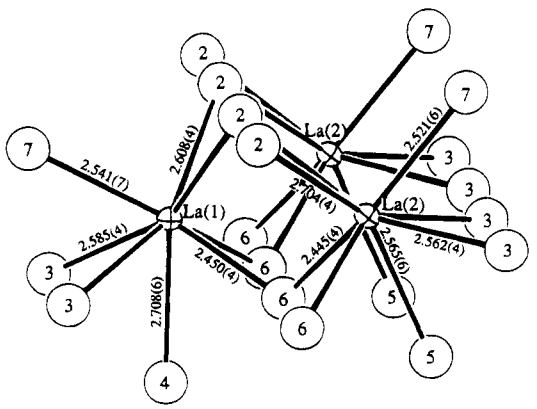

Figure 4. ORTEP drawing of three eight-coordinated LaO_8 bicapped trigonal prisms. A common edge made of O(2) and O(6) is shared by the trigonal prisms of the two crystallographically independent La(1)-O_8 and La(2)O_8 btp's. The anisotropic La atoms are presented at 90% probability. The numbered circles, drawn in an arbitrary size, represent oxygen atoms. The bond distances are in Å.

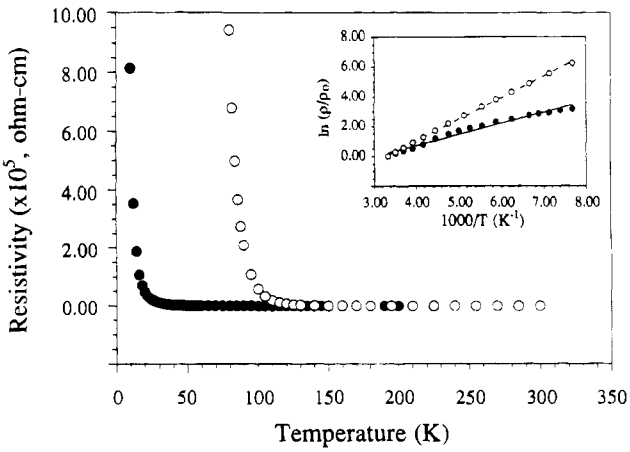

Figure 5. Resistivity (Ω m) vs temperature (K) plot of pressed pellet samples of $La_4Ti_5Si_{4-x}P_xO_{22}$ ($x = 0$ (solid dots), 1 (open circles)). The insert is the corresponding $\ln(\rho/\rho_0)$ vs $1000/T$ (K^{-1}) plot. The straight lines are drawn to show the linearity.

The variable-temperature transport properties, as shown by the resistivity curves in Figure 5, of both oxosilicate and mixed-oxosilicophosphate compounds, $La_4Ti_5Si_{4-x}P_xO_{22}$ ($x = 0$, 1), have been evaluated by the electrical resistivity measurements

of pressed pellet samples. The measured room-temperature resistivities are moderately high, 8.9 and 6.3 Ω cm, respectively, which suggests that these materials are poor conductors. The observed sharp resistivity transitions, occurring at 13 K (x = 0) and 90 K (x = 1), indicate a possible transitional insulating state at low temperatures. The $\ln(\varrho/\varrho_o)$ vs $1/T$ plot, presented in the insert, for the temperature range 130−300 K, shows a nearly linear relationship; this behaves as is expected for a semiconductor. The calculated gap energy (E_g), according to the equation $\ln(\varrho/\varrho_o) = E_g/2kT$ (where ϱ/ϱ_o is the relative resistivity ratio, $k = 8.62 \times 10^{-5}$ eV K^{-1}), shows a small gap energy, ca. 0.13 and 0.25 eV, respectively. From these observations, questions have been raised concerning the normal state electronic structure at the valence region as well as the nature of the ground state electronic interactions above and below the transition.

Although, at beginning of our investigation, a metallic state was considered on the basis of direct Ti−Ti interactions that occur across the shared edge of the octahedral chains, the resulting small gap energies and sharp transitions corresponding to nonmetallic characteristics are not entirely unexpected. According to the studies of extended Hückel tight-binding (EHTB) calculations,[22] the d-block band at the valence region consists of the d orbitals of the rutile slab and is partially filled. Also, the Ti(1) d orbitals are well above the Fermi level. The formal oxidation states, in terms of the charge distribution, in the oxosilicate compound can, thus, be assigned as $[La_4Ti^{4+}(Si_2O_7)_2](TiO_2)_4^{4-}$, where the titanium cations in the rutile layer possess an average oxidation state of 3+.[23] This, in fact, results in a situation similar to the d^1 electronic state in VO_2. In the latter, the $3d^1$ V^{4+} cations have been observed to be covalently bonded in V pairs which is known as Mott insulator.[24] Therefore, the observed semiconducting behavior can be rationalized to be a result of pairing or bond formation to avoid repulsive near-neighbor electron interaction. In the phosphorus substituted mixed-oxosilicophosphate (x = 1) phase, the ground state energy is presumably further lowered through enhanced Ti−Ti interaction attributed to the increased electron concentration, and hence, a higher gap energy and increased transition temperature are observed. This implies that the mechanism with regards to the transition is quite similar to that in the titanium oxide Ti_4O_7, whose nonmetallic state below 150K is associated with a bipolaron formation.[25] Detailed discussions concerning the EHTB analyses of the $[La_4Ti(Si_2O_7)_2](TiO_2)_{4m}$ series will be presented in a later report.

Conclusion

During the systematic search for transition metal oxo compounds, a mixed-valence titanium(III/IV) compound $La_4Ti_5Si_4O_{22}$ has been isolated from a high-temperature solid-state reaction via the molten $BaCl_2$ flux. The crystal structure of $La_4Ti_5Si_4O_{22}$ is the chevkinite type determined for the first time. The new oxosilicate compound represents the first member (m = 1) of the $La_4Ti(Si_2O_7)_2(TiO_2)_{4m}$ series, whose structure is characterized by the intergrowth of the $La_4Ti(Si_2O_7)_2$ and TiO_2 sublattices. The newly developed $La_4Ti_5Si_{4-x}P_xO_{22}$ family lends additional merit, in terms of varying the electron counts, to the systematic study of electron behavior concerning the metal−insulator transitions commonly seen in the d^1 transition metal oxide systems. Although a conduction mechanism with regards to the sharp resistivity transitions has been suggested, further studies aimed toward conclusive evidences for bipolaron formation are necessary and await the growth of large single crystals. Finally, the compound series is unique in the sense that the two-dimensional structures can be viewed as a rutile lattice that is sliced along the [110] plane by the silicate slabs into various sized (m) TiO_2 layers. The demonstrated example shows that a new compound class can be made, in which the interesting metal−insulator transitions and associated physical phenomena previously observed in the early transition metal oxide systems can be investigated in a confined space.

Acknowledgment. Acknowledgment is made to the National Science Foundation (Grant DMR-9208529), the Robert A. Welch Foundation and the Exxon Education Foundation. The authors are also indebted to Professor M.-H. Whangbo for the EHTB calculations and valuable discussions concerning the resistivity results. Financial support for the single-crystal X-ray diffractometer by the NSF is also acknowledged.

Supplementary Material Available: Tables of detailed crystallographic data and anisotropic thermal parameters (2 pages). Ordering information is given on any current masthead page.

IC940966+

(22) Wang, S.; Hwu, S.-J.; Paradis, J. A.; Whangbo, M.-H. *Inorg. Chem.*, to be submitted for publication.

(23) Excluding the bond valence contribution due to the close Ti−Ti interaction, the bond valence sum calculations using observed Ti−O distances give rise to a set of oxidation states for the Ti cations—$V_{Ti(1)}$ = 3.17 v.u., $V_{Ti(2)}$ = 3.47 v.u., $V_{Ti(3)}$ = 3.41 v.u., $V_{Ti(4)}$ = 3.38 v.u.—and in turn a slightly different charge distribution assignment: $[La_4Ti^{3+}(Si_2O_7)_2](TiO_2)_4^{3-}$. The detailed discussions will be reported in ref 22.

(24) (a) Pouget, J. P.; Launois, H.; Rice, T. M.; Dernier, P.; Gossard, A.; Villeneuve, G.; Hagenmuller, P. *Phys. Rev. B* **1974**, *10*, 1801−15. (b) Brandow, B. H. *Adv. Phys.* **1977**, *26*, 651−808. (c) Whangbo, M.-H. *J. Chem. Phys.* **1979**, *70*, 4963−6.

(25) (a) Lakkis, S.; Schlenker, C.; Chakraverty, B. K.; Buder, R.; Marezio, M. *Phys. Rev. B* **1976**, *14*, 1429−40. (b) Chakraverty, B. K.; Schlenker, C. *J. Phys.(Les Ulis, Fr.)* **1976**, *37*, C4, 353−6. (c) Schlenker, C.; Marezio, M. *Philos. Mag. B* **1980**, *42*, 453−72.